

# Mixing Atomistic and Coarse Grain Solvation Models for MD Simulations: Let WT4 Handle the Bulk

Leonardo Darré,<sup>†</sup> Alex Tek,<sup>‡,§</sup> Marc Baaden,<sup>\*,‡</sup> and Sergio Pantano<sup>\*,†</sup>

<sup>†</sup>Institut Pasteur de Montevideo, Mataojo 2020, CP 11400, Uruguay

<sup>‡</sup>Laboratoire de Biochimie Théorique, CNRS, UPR9080, Univ Paris Diderot, Sorbonne Paris Cité, 13 rue Pierre et Marie Curie, 75005, Paris, France

<sup>§</sup>Université Pierre et Marie Curie, UPMC Sorbonne Universités, 4 place Jussieu 75005 Paris, France

## Supporting Information

**ABSTRACT:** Accurate simulation of biomolecular systems requires the consideration of solvation effects. The arrangement and dynamics of water close to a solute are strongly influenced by the solute itself. However, as the solute–solvent distance increases, the water properties tend to those of the bulk liquid. This suggests that bulk regions can be treated at a coarse grained (CG) level, while keeping the atomistic details around the solute. Since water represents about 80% of any biological system, this approach may offer a significant reduction in the computational cost of simulations without compromising atomistic details. We show here that mixing the popular SPC water model with a CG model for solvation (called WatFour) can effectively mimic the hydration, structure, and dynamics of molecular systems composed of pure water, simple electrolyte solutions, and solvated macromolecules. As a nontrivial example, we present simulations of the SNARE membrane fusion complex, a trimeric protein–protein complex embedded in a double phospholipid bilayer. Comparison with a fully atomistic reference simulation illustrates the equivalence between both approaches.

## INTRODUCTION

Molecular dynamics (MD) simulations are nowadays a reliable and well-established alternative to obtain atomic details on the structural and dynamic properties of molecular systems for which experimental data are difficult or impossible to acquire. However, owing to high computational cost, the time and size scales currently affordable by MD techniques fall very often short when compared with those that are experimentally relevant. This is particularly the case for simulations of biological systems. An increasingly adopted shortcut for this problem is the use of simplified or coarse grained (CG) molecular representations, where groups of atoms are replaced by effective interacting sites.<sup>1–9</sup> Although these approaches effectively achieve a sensible rise in the sampling time, the inherent loss of resolution may sometimes compromise their use. For instance, the role played by the discrete nature of water molecules in forming or disrupting hydrogen bonds, forces resulting from hydrophobic interactions, electrostatic screening, etc., are difficult to reproduce with CG approaches. Since water constitutes, on average, 80% of biological systems, dual resolution approaches where a solute and water in its close neighborhood are treated at atomistic or fine grain (FG) detail and the more remote bulk solvent is represented at the CG level may be very advantageous in reducing the number of particles to be treated without compromising accuracy. Some examples reported in the literature suggest that these hybrid or multiresolution techniques constitute a practical alternative to reach the various size and time scales involved in complex biomolecular systems, keeping the atomic detail in the solute.<sup>5,10–13</sup> To a first approximation, two main methodological trends can be distinguished: variable resolution and fixed resolution. The first strategy allows for a change in the degree

of representation *on the fly* along the simulation.<sup>14,15</sup> The molecular system is usually divided in three regions: FG, hybrid FG–CG, and CG. Particles change their resolution when they cross from one region to another. The transition between these regions is ruled by a scaling function that interpolates the interaction forces or potentials between the FG and CG regions, according to the position of the particles in space. A hybrid region is often required to smooth the potential and kinetic energy of the system when groups move from the CG to the FG region or *vice versa*.<sup>16,17</sup>

In the second method, the representation level of each particle (i.e., either CG or FG) is fixed at the beginning of the simulation and remains unaltered. This approach has the advantage that no position dependent transformations are required.

A crucial point in multiresolution methods regards the derivation of the mixed FG–CG cross-interactions. Since CG objects are not necessarily real physical entities, the FG–CG interaction may not correspond to a physical one. Therefore, a manifold of different and equally valid strategies for their derivation can be found in the literature. For example, Michel et al.<sup>18</sup> developed a CG model for lipids compatible with the CG water model called Soft Sticky Dipole (SSD).<sup>19</sup> In this case, the FG–CG interactions were adjusted to reproduce water/octane partitioning coefficients.

From a different perspective, Shi et al.<sup>20</sup> systematically derived FG–CG interaction parameters using a force matching

**Special Issue:** Wilfred F. van Gunsteren Festschrift

**Received:** March 3, 2012

**Published:** June 4, 2012



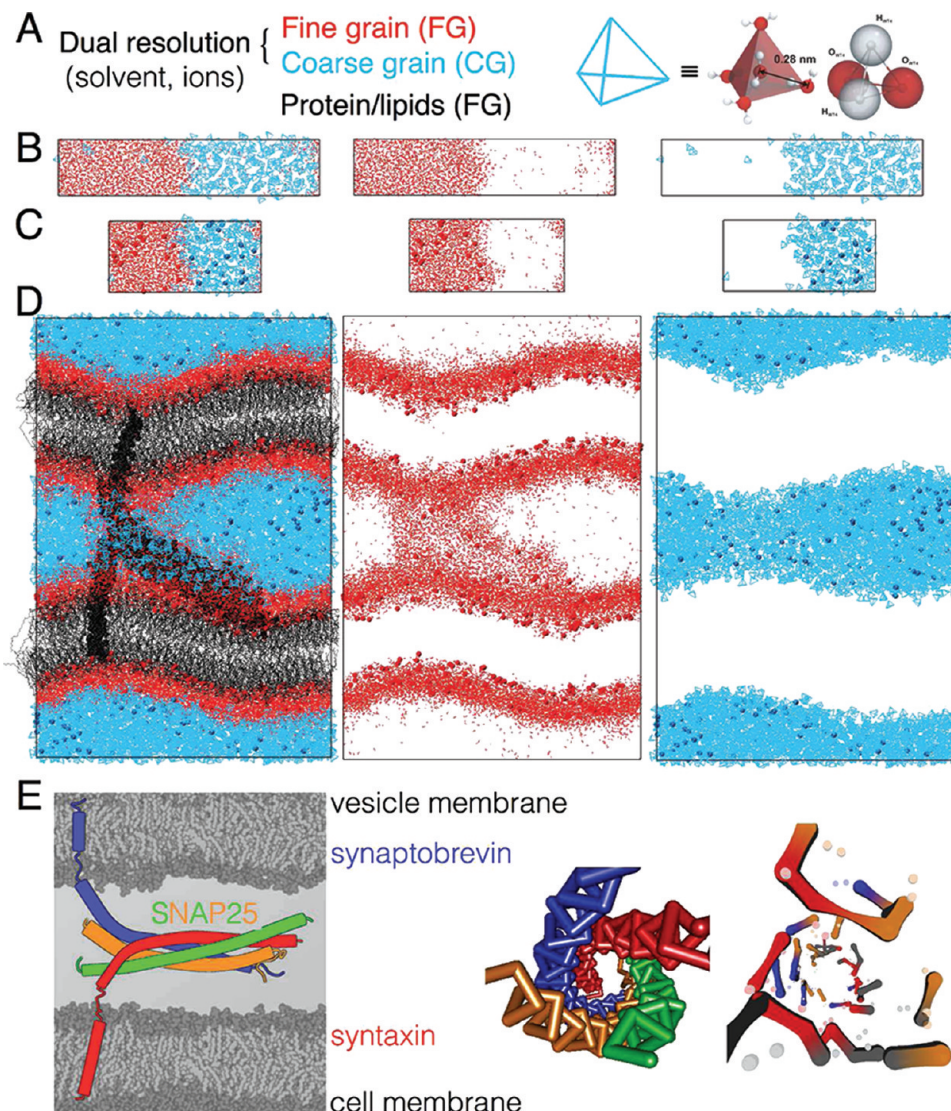


**Figure 1.** Schematic representation of the molecular systems studied. (A) Illustration of the WT4 CG water model. (B) System used to study the properties of pure water. The middle and right panels show the FG and CG phases separately. Red and cyan colors are used to indicate the FG and CG particles, respectively. (C) Representation of the system used to study the properties of electrolyte solutions. (D) Protein/double membrane system used as test case for the hybrid solvation approach. Gray and black colors are used to represent phospholipids and proteins, respectively. (E) A schematic view of the SNARE complex bundle is shown on the left. A view down the bundle axis is shown in the center, and some of the salt bridge interactions that hold it together are depicted on the right. The latter parts of the figure were prepared with the HyperBalls tool.<sup>71</sup>

approach. In this scheme, FG interactions remain unchanged with respect to FG simulations used as a reference; effective pairwise CG interactions were derived directly from trajectory and force data from the reference MD simulations.<sup>21</sup> To derive the FG–CG interactions, the FG and CG forces were subtracted from the reference forces in the FG simulation, and FG–CG interactions were obtained by fitting the residual forces.

As a final example, Rzepiela and co-workers addressed a hybrid representation of liquid butane by modeling atomistic molecules carrying virtual interaction sites at the center of mass of each molecule.<sup>22</sup> Through these sites, FG molecules interact with the CG neighbors *via* previously determined CG potentials. The force from CG interactions acting on a virtual site is spread over the corresponding atoms as a mass weighted fraction of the total force acting on the virtual site. This solution avoids the use of specific FG/CG interactions, granting the method a general transferability and independence between

FG and CG force fields. However, a quantitative description of solvation effects on dianiline molecules is only captured if a continuous dielectric constant is used as a free fitting parameter.<sup>22</sup>

In this contribution, we present a dual resolution model for aqueous solvation belonging to the second approach (fixed resolution). It is based on the combined use of the popular SPC water model<sup>23</sup> together with our recently developed CG model for water, called WatFour (WT4, for shortness<sup>24</sup>). In this CG model, four linked beads are placed at the corners of a regular tetrahedron whose geometry corresponds to that of the tetrahedral structure of water (Figure 1A). The interactions in the WT4 model (bonding, van der Waals, and electrostatics) are calculated within the same Hamiltonian function and combination rules used in FG simulations. Hence, if a number of SPC and WT4 water molecules are mixed in a simulation box, it is possible to obtain a simultaneous description of FG and CG regions without the need for specific terms describing

**Table 1. List of Systems and Simulation Conditions**

system number	components and number of atoms (N.At.)	ionic concentration [M]	temperature [K], thermodynamic ensemble, and pressure coupling	simulation time [ns]	calculated properties
1 (FG)	SPC (4004) N.At. <b>12012</b>	...	300, 298, 318 NPT, isotropic	5, 1, 1	density, Kirkwood factors, relaxation time, relative permittivity, diffusion coefficient, isothermal compressibility, heat capacity, expansion coefficient
2 (hybrid)	SPC (2002), WT4 (182) N.At. <b>6734</b>	...	300, 298, 318 NPT, isotropic	5, 1, 1	density, Kirkwood factors, relaxation time, relative permittivity, diffusion coefficient, isothermal compressibility, heat capacity
3 (hybrid)	SPC (4565) WT4 (153) N.At. <b>14307</b>	...	300 NVT	3	density, Kirkwood factors, relaxation time, relative permittivity, diffusion coefficient, isothermal compressibility, heat capacity, surface tension
4 (hybrid)	SPC (2002), Na <sup>+</sup> (10), Cl <sup>-</sup> (10) N.At. <b>6206</b>	0.3	300 NPT, isotropic	10	number density, ion–water RDF and cation–anion RDF, water coordination number, self-diffusion coefficient
5 (hybrid)	SPC (2002), Na <sup>+</sup> (10), Cl <sup>-</sup> (10), WT4 (160), NaW <sup>+</sup> (10), ClW <sup>-</sup> (10) N.At. <b>6206</b>	0.3	300 NPT, isotropic	10	number density, ion–water RDF and cation–anion RDF, water coordination number, self-diffusion coefficient
6 (FG)	SPC (7612), Na <sup>+</sup> (34), Cl <sup>-</sup> (34) N.At. <b>22904</b>	0.25	300 NVT	10	osmotic pressure
7 (hybrid)	SPC (7612), Na <sup>+</sup> (34), Cl <sup>-</sup> (34), WT4 (649), NaW <sup>+</sup> (34), ClW <sup>-</sup> (34) N.At. <b>25568</b>	0.25	300 NVT	10	osmotic pressure
8 (FG)	protein complex, <sup>a</sup> POPC(1008), POPS (123), SPC (80453), Na <sup>+</sup> (328), Cl <sup>-</sup> (198) N.At. <b>304564</b>	0.1 <sup>b</sup>	310 NPT, semi isotropic in the membranes' plane	64 (last 15 used for analysis)	full system: density profiles membrane:bilayer thickness, intermembrane distance, area per lipid, PN angle, order parameter protein: RMSD, RMSE, structural superposition, salt bridges, hydrogen bonds, distance maps
9 (hybrid)	protein complex, <sup>a</sup> POPC(1008), POPS (123), SPC (28973), Na <sup>+</sup> (215), Cl <sup>-</sup> (68), WT4 (4680), NaW <sup>+</sup> (113), ClW <sup>-</sup> (130) N.At. <b>168844</b>	0.1 <sup>b</sup>	310 NPT, semi isotropic in the membranes' plane	20 (last 15 used for analysis)	full system: density profiles, membrane:bilayer thickness, intermembrane distance, area per lipid, PN angle, order parameter protein: RMSD, RMSE, structural superposition, salt bridges, hydrogen bonds, distance maps

<sup>a</sup>Chain A: Synaptobrevin (sb, aa: 1–92). Chain B: Syntaxin (sx, aa: 93–195). Chain C: SNAP25 (aa: 196–346). Notice that these residue numbers correspond to the numbering in the simulation systems and not the actual protein sequence. <sup>b</sup>Not considering 130 neutralizing counterions (Na<sup>+</sup>).

FG–CG interactions. Owing to the differences in their respective free energies of solvation, the FG–CG mixture separates in two phases at room temperature.<sup>25</sup>

Underlying this work is the idea that an atomistic solute offers pinning sites when solvated with fully atomistic water. These sites modify the structure and dynamics of a proximal shell of solvent molecules.<sup>26,27</sup> Water molecules beyond this solvation shell recover bulk properties, in line with the observation that water dynamics is predominantly influenced by the presence of the first and second solvation shells.<sup>28</sup> Therefore, it may be possible to treat those bulk solvent molecules at a CG level. To test this hypothesis, we will analyze different situations involving the mixing of SPC and WT4 water models. The attention will be focused on the possible perturbations introduced by the CG molecules onto the FG reference phase.

With the aim of applying our approach to complex biological models, we will analyze two simple aqueous systems to characterize the intrinsic properties of dual-resolution SPC/WT4 systems, before treating a realistic test case involving membranes and proteins (Figure 1). The first system represents pure water modeled as a mixture of SPC and WT4 molecules (Figure 1B). The second one further includes simple electrolytes in the solution (Figure 1C). Finally, as test case for a biological system, we use a model of the SNARE complex (acronym derived from “Soluble NSF Attachment Protein Receptor”). This model represents the minimal membrane fusion machinery.<sup>29</sup> It is composed of the proteins syntaxin, synaptobrevin, and SNAP-25 arranged in a cytoplasmic four-helical protein bundle attached to two transmembrane segments, which are inserted in a double phospholipid bilayer (Figure 1D,E). We previously set up and equilibrated an initial model.<sup>30</sup> Here, we compare an atomistic simulation starting from the previously equilibrated model with a dual-resolution setup. Such a complex system provides a critical assessment and sensible probe for alterations induced by mixing resolutions. No significant differences were observed, and the comparisons of the simulation performed at full FG level with the FG–CG scheme for the solvent indicate that most properties are conserved to statistical precision.

## COMPUTATIONAL DETAILS

Several aqueous solution systems were simulated to test our dual-resolution solvation scheme. The composition of the systems tested, simulation times and conditions, temperatures, and calculated properties are listed in Table 1.

All MD simulations were performed using the GROMACS 4.5 software with a time step of 2 fs. The LINCS algorithm<sup>31</sup> was applied to all bonds connecting hydrogen atoms, and SETTLE<sup>32</sup> was used for SPC water. Temperature and pressure were kept constant using the Berendsen thermostat and barostat,<sup>33</sup> with coupling times of 0.1 and 0.5 ps, respectively. For systems 1 to 9, a cutoff for nonbonded interactions of 1.2 nm was used, while long-range electrostatics were taken into account using the particle mesh Ewald approach.<sup>34,35</sup> All interactions, FG–FG, CG–CG, and FG–CG, were straightforwardly calculated within the pairwise Hamiltonian of GROMACS 4.5.

Solvation free energy calculations were performed for SPC and WT4, using first SPC and then WT4 as a solvent. In each case, the chosen water molecule was placed in a box filled with FG or CG solvent, and the interaction of the former with its surrounding medium was gradually turned off. For this purpose,

the nonbonded interactions of the water molecule with the solvent were coupled with a scaling factor  $\lambda$  that goes from 0 (full interaction) to 1 (null interaction). In our case, we used a sequence of 21 equally spaced steps (increments of 0.05). For each of these  $\lambda$  values, energy minimization and equilibration preceded a 5 ns NVT molecular dynamics simulation from which the average value of the derivative of the potential energy with respect to the scaling factor ( $\langle \delta V / \delta \lambda \rangle$ ) was obtained. Because the free energy difference of the process is the integral from 0 to 1 of the expectation value of  $\delta V / \delta \lambda$  calculated for each  $\lambda$ , we obtained the free energy of solvation by numerically integrating those values.

Density profiles, self-diffusion coefficient, rotational relaxation time, permittivity, and Kirkwood factor were obtained using standard GROMACS tools. The self-coordination number was computed by counting the number of SPC oxygen atoms and WT4 beads contained in a sphere with a 0.55 nm radius (first and second solvation shells). The g\_rdf tool of GROMACS was used to compute the number density around SPC oxygen atoms (O–O calculated on FG molecules surrounding SPC oxygen atoms and O–WT4 calculated on the WT4 beads). The total number density distribution was obtained by summing both number densities, multiplying the O–WT4 one by 2.8, according to the CG factor of the WT4 beads.<sup>24</sup> To obtain the normalized radial distribution function (RDF), the total number density was divided by the value of this function taken at a point where convergence was achieved. In our case, this value was taken at a distance of 1.5 nm from the origin.

Isothermal compressibility was calculated evaluating the fluctuations of the volume on system 1, according to the procedure reported by Herrero.<sup>36</sup> Surface tension was evaluated as in ref 37 on system 2. The expansion coefficient and the heat capacity were calculated following the procedure reported in ref 38. The calculation of the osmotic pressure was based on the methodology presented by Luo and Roux,<sup>39</sup> using the implementation reported in ref 24.

For the simulation of the SNARE complex, we used a previously set up full atomistic model in explicit solvent, inserted into two fully hydrated mixed lipid bilayers consisting of 1-palmitoyl-2-oleoyl-phosphatidylcholine (POPC) and 1-palmitoyl-2-oleoyl phosphatidylserine (POPS). The construction process of this reference model is described in detail in ref 30. The mixed bilayer system with 11% POPS and a 0.1 mol/L NaCl solution was equilibrated during 44 ns of molecular dynamics simulation as previously described. The GROMOS-87 force field<sup>40</sup> with additional POPS parameters<sup>41</sup> was used. Production continuation runs were carried out for 20 ns, discarding the first 5 ns for equilibration of the corresponding dual-resolution simulation, using periodic boundary conditions and full electrostatics with the particle mesh Ewald (PME) method,<sup>34,35</sup> with a direct space cutoff of 1 nm. The translational center of mass motion was removed every step.

To test our dual-resolution solvation model, we set up a system analogous to system 8 with hybrid solvation (system 9 in Table 1). The construction procedure was the following: We took the last snapshot of the MD simulation of system 8 after 44 ns. In this conformer, all water molecules beyond 1 nm of any protein or membrane atom were removed. The remaining empty space was filled with WT4 molecules. The coordinates were taken from a prestabilized box containing 16 WT4 molecules. Finally, the FG ions, which remained in the CG phase, were replaced by their corresponding CG ion counter-

parts. Energy minimization and 5 ns of equilibration were conducted previous to the production simulation.

Several properties were measured in order to account for the ability of the hybrid solvent to mimic a full FG one. Membrane properties were calculated on the entire system (curved membrane) and on a straight patch of 3 nm by 10 nm, which is not in contact with the protein during all of the simulation. Density profiles of the components of the system were calculated in the direction perpendicular to the membrane. The intermembrane distance was calculated in two dimensions to account for perturbations induced by the transmembrane domains of the protein complex. We averaged the distances between lipid heads of the two outer leaflets along the  $z$  axis over time using a grid of 0.5 nm spacing in the  $xy$  plane. Order parameters of the lipids were calculated as the angle between the hypothetical carbon–deuterium bond and the  $z$  axis ( $S_{CD}$ ).<sup>42</sup> The orientation of the P–N vectors was measured as the angle between the line connecting the amino and phosphate groups and the normal of the bilayer.

The root mean square deviation (RMSD) and fluctuation (RMSF) were calculated on the  $C\alpha$  atoms along the trajectory. Intra- and intermolecular hydrogen bonds were taken into account within cutoff distances and angles of 0.35 nm and 35°, respectively, while a 0.5 nm distance cutoff between oppositely charged side chains was used to detect salt bridges.

Contacts between different molecular species were considered up to a distance of 0.4 nm.

## RESULTS

Our approach for hybrid FG–CG solvation of biomolecular systems is based on the mixture of two models representing water at different description levels. A mixture of SPC and WT4 models may accelerate sampling in MD simulations since bulk water can be represented by WT4 molecules, reducing the number of particles by a factor of 2 or more. The implementation of the scheme is straightforward since all of the interactions are calculated simultaneously using the same Hamiltonian form.

In order for this approach to work, the reciprocal free energies of solvation of both models should determine the (at least partial) separation in two phases. If this is achieved, the FG water should remain in the surroundings of the FG solute and the CG molecules should remain in the bulk. Furthermore, not only should such partitioning occur but also the physicochemical features of the different components of the systems should remain the same as those of a homogeneous FG system.

We first sought to calculate the free energies of solvation of a single SPC molecule within a box of pure WT4 liquid and *vice versa*.<sup>25</sup> For partitioning to occur spontaneously in such systems, the free energy of solvation of SPC in SPC should be lower than the one for SPC in WT4, and *vice versa* for WT4. Table 2 reports the result of such free energy computations,

**Table 2. Free Energies of Solvation of FG, CG, and Hybrid Water Models**

solute	solvent	$\Delta G_{\text{solv}}$ [kJ/mol]
SPC	SPC	-36.8
SPC	WT4	-13.2
WT4	SPC	-35.6
WT4	WT4	-50.7

confirming that phase separation is thermodynamically favored. Moreover, the negative values obtained in all cases indicate that both molecular species are soluble in both liquids. This suggests that our approach may effectively lead to a practical hybrid solvation approach to speed up MD simulations without a sensible loss in atomistic accuracy.

In the next sections, we will present some common physicochemical properties of the hybrid liquid in comparison to atomistic ones. Section 1 addresses the properties of the pure water in hybrid representation, compared against a pure SPC simulation and experimental data. Section 2 introduces the hybrid treatment of free electrolytes, and some properties of ionic solutions are compared against pure FG simulations. Finally, section 3 presents a systematic comparison of structural and dynamic features of the SNARE membrane fusion complex simulated with pure FG and hybrid solvation in order to validate the present approach for large and biologically relevant systems.

Whenever we address the hybrid system, it is important to keep in mind that each WT4 molecule represents 11 FG water molecules while every CG ion represents the corresponding FG ion plus six FG water molecules.<sup>24</sup> In that sense, whenever we refer to the *total* number of solvent molecules, the sum of the FG water and ions plus 11 water molecules per each WT4 and an ion plus six water molecules per each CG ion is considered.

**1. Pure Water.** Thermodynamic data presented above predict that a mixture of SPC and WT4 water should partition in two phases. In order to study the behavior of such a mixture, we ran molecular dynamics simulations in the NPT ensemble at 300 K and 1 bar using a box containing two apposed slabs of 2002 SPC molecules and 182 WT4 molecules (system 1, Figure 2A). Since each WT4 molecule represents 11 waters, this system can be regarded as a 1:1 mixture of FG and CG water molecules.

All of the results described hereafter refer to this configuration. Nevertheless, none of the calculated properties change if the starting configuration is fully mixed. The final configuration of such starting conditions results in well partitioned phases already after the thermalization/pressurization period (see Figure S1, Supporting Information). However, it is difficult to identify a preferential axis in such a configuration. Therefore, a starting configuration such as that shown in Figure 2A was chosen for the sake of visual clarity and easier interpretation.

The degree of mixing of both water representations can be evaluated from the time averaged mass density along the direction perpendicular to the SPC-WT4 interface (Figure 2B). Clearly, hybrid water under room conditions partitions in two phases. The FG and CG phases do not create a sharp interface. Both density traces undergo a smooth transition along the longitudinal axis describing a nearly sigmoid shape (Figure 2B). The transition from minimum to maximum values takes place within a distance of almost 2 nm. However, none of the curves reaches either the maximum density value expected for a pure system nor zero, showing that a small number of SPC and WT4 molecules penetrate within their opposite phase. This shift is evident from the comparison with the density calculated for system 2, which contains only pure SPC molecules. The black trace on the left of Figure 2B shows the density corresponding to the pure FG system, which remains slightly above that of SPC water in the hybrid system. However, very good agreement is found considering the total number of waters represented by the sum of SPC and WT4 molecules within the

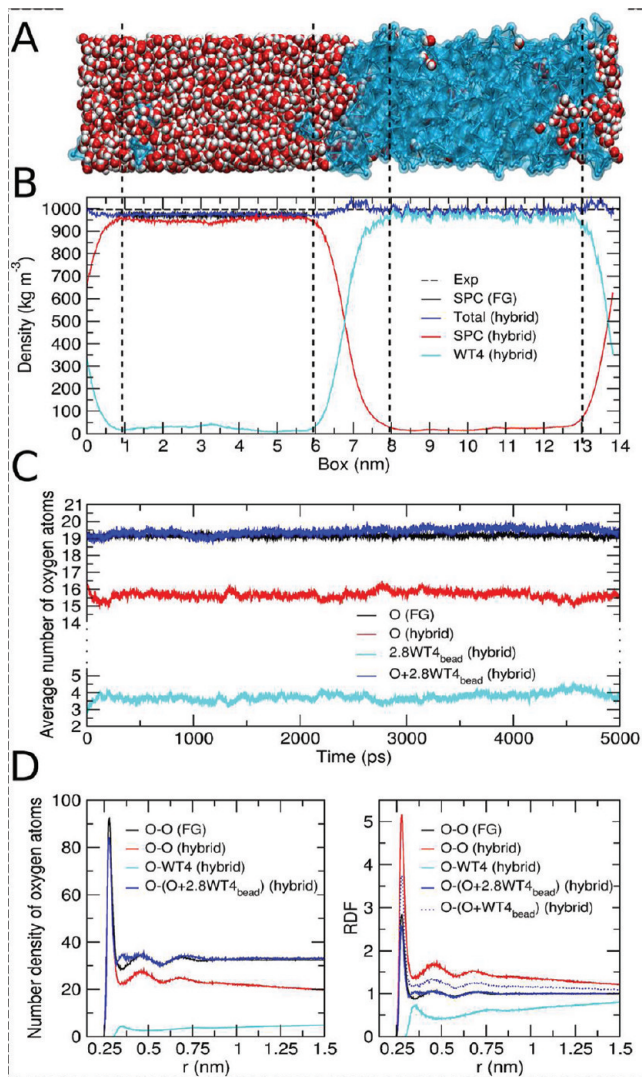


**Figure 2.** Pure water systems. (A) Snapshot of system 2 after 5 ns of molecular dynamics simulation. Red and white vDW representation, SPC water; cyan CPK/surface representation, WT4. (B) Mass density profile along the direction orthogonal to the FG/CG interface for system 2. Comparisons with respect to an equivalent FG simulation (system 1) and experimental data are shown. Vertical dashed lines indicate the limits between FG/interface and CG/interface regions. Panels A and B are on the same scale. (C) Water self-coordination number. Time series of the number of oxygen atoms at 0.55 nm from the oxygen of any water is shown for the FG reference simulation (system 1) and hybrid simulation (system 2). (D) O-O number density (left) and O-O radial distribution function (right) measured on FG reference system 1 are compared against hybrid system 2.

atomistic side of system 1. This is not surprising if we consider that the WT4 model mimics the tetrahedral structure of bulk water. As could be anticipated, WT4 molecules may intercalate within SPC water by substituting small water clusters without perturbing its global structure. This suggests that both molecular species may cross the interface with a modest energetic cost. As a result, the total density of the CG compartment reproduces that of experimental water, although with more noise because of the higher granularity of the medium. A small overestimation ( $\sim 3\%$  with respect to the experimental value) is only observed within the interface. This increase in the density is ascribed to a slightly higher occupation of SPC and WT4 species within intermolecular

interstices of the liquid. Hence, despite such minor interface artifacts, the density profile of both FG and CG regions is not altered by the hybrid scheme.

A gauge on the stability of the mixture can be obtained from the temporal evolution of the self-coordination number for oxygen atoms within a sphere of 0.55 nm (Figure 2C). This distance includes the first and second solvation shells, providing a rather accurate measure of possible spurious effects of the method. In the case of the hybrid system, the coordination number was computed for SPC, for the total water molecules represented by WT4, and for the sum of both.

A certain increase in the degree of mixing is observed during the first 200 ps. This is evident from the decrease in the coordination number of FG water oxygens and the increase in the number of total or effective oxygens represented at the CG level (bottom and medium traces in Figure 2C, respectively). This analysis suggests that molecules at the interface start to mix immediately after the beginning of the simulation. A small amount of each class of these molecules diffuses reaching the opposite phase. This exchange process stabilizes rapidly since no drift in the coordination number is observed after the first  $\sim 200$  ps, attesting to the temporal stability of the FG–CG mixing behavior.

The global coordination number of SPC water in the hybrid scheme (system 1) is, obviously, smaller than that calculated for the FG case (system 2) owing to the presence of CG molecules (Figure 2C). However, when the total number of waters represented by the CG molecules is calculated, the coordination numbers from systems 1 and 2 show very good agreement with maximum differences on the order of or below 3% (top traces in Figure 2C).

In order to characterize the structural arrangement of water, we calculated the number density around SPC oxygen atoms. The comparison between FG and hybrid systems provides some interesting insights into the structural arrangement of the solvent. Both oxygen–oxygen (O–O) number densities show good agreement in the radial position of the solvation shells between systems 1 and 2 (Figure 2D, left panel). The height of the function is progressively underestimated with the increase of the radial distance in relation to the pure FG water, owing to the presence of WT4 molecules beyond the hybrid interface. If we focus on the arrangement of the CG beads around the FG oxygen, the first shallow peak appears at  $\sim 0.35$  nm from atomistic oxygens. After that point, we observe a smooth monotonic increase that mirrors the decrease of O–O number density. This suggests that CG water has a small effect on the arrangement of neighboring FG species. A constant behavior is recovered if the total number of waters is taken into account (considering that each WT4 bead represents 2.8 water molecules, Figure 2D). This indicates good agreement with the FG simulation. It should be noted that the curve relaxes and no signs of freezing (related to long-range periodicity) are observed. The major differences from the pure atomistic case remain a small difference in the height of the peak corresponding to the first solvation shell and the presence of the shallow spurious maximum between the first and second solvation shells. The cause of both effects is the position of WT4 beads, which is shifted in the outward direction in reference to the first solvation shell of FG water. However, as will be shown in the forthcoming paragraphs, few or no deviations are found in the physicochemical characteristics reproduced by the hybrid solvent in reference to experimental values.

Table 3. Comparison of Physicochemical Properties of Pure Water

	Kirkwood factor <sup>a</sup>	relaxation time ( $\tau^{\text{HH}_2}$ / $\tau^{\text{OH}_2}$ ) [ps]	relative permittivity	diffusion coeff. [ $\times 10^{-5} \text{ cm}^2 \text{ s}^{-1}$ ]	isothermal compressibility [GPa <sup>-1</sup> ]	heat capacity [kJ mol <sup>-1</sup> K <sup>-1</sup> ]	surface tension [mN m <sup>-1</sup> ]
SPC	2.53	1.0/0.9	65	4.3	0.534 <sup>38</sup>	0.074 <sup>38</sup>	53.4 <sup>37</sup>
Hybrid SPC/WT4	2.9	1.2/1.0	84	2.9	0.52	0.043	52
WT4	— <sup>b</sup>	— <sup>b</sup>	110	2.23	2.43		17
Exp.	2.9 <sup>43</sup>	1.95 <sup>44</sup>	78.4 <sup>45</sup>	2.27 <sup>46</sup>	0.46	0.075 <sup>c</sup>	71.2 <sup>47</sup>

<sup>a</sup>Calculated after 5 ns of simulation. <sup>b</sup>Kirkwood factors and relaxation times cannot be calculated for WT4 molecules. <sup>c</sup>Taken from ref 38.

Notice that we have referred to the number density instead of the commonly used oxygen–oxygen radial distribution functions (O–O RDF). The RDF is a measure of the probability to find a given number of particles around a reference point when increasing the radial coordinate. The proper normalization of this function requires taking into account the increasing dimension of the spherical shell with the radial distance and the density at the bulk. In the case of a hybrid solvation approach, a proper normalization to the bulk density is not possible if the density of the particles changes at the interface and thereafter. In our case, if the distribution is wrongly normalized setting a unitary value for the bulk density, the obtained RDF is overestimated (Figure 2D, right panel). A workaround for this is to calculate the RDF of both molecular species separately, add them up using the correct coarse graining factor (2.8 in our case), and use the value of the density at a point after which the curve relaxes as the normalization factor (see Computational Details). If this procedure is followed, the RDF function obtained compares very well with its purely atomistic counterpart (Figure 2D, right panel).

Besides RDF, the structural arrangement of a polar liquid can be characterized by the dipole–dipole correlation between water molecules. This can be achieved by the calculation of the Kirkwood factors ( $g_k$ ) for infinite systems. For nonpolar or moderately polar liquids,  $g_k$  is not expected to deviate significantly from unity, as nonpolar solvent molecules do not impose a preferential orientation to their neighbors. However, for hydrogen-bonded liquids, such as water,  $g_k$  deviates considerably from one. This is related to the strong influence of hydrogen bonds on the relative orientation of molecules in the liquid. The calculated  $g_k$  for SPC water, which is in agreement with previous reports,<sup>38</sup> yields a slight underestimation with respect to the experimental data (2.90<sup>43</sup>). However, Kirkwood factors calculated for the hybrid system show an increase, which coincides with the experimental data (Table 3).

On the basis of this result, we assess whether the dielectric properties of the hybrid liquid, as a whole, are well reproduced. In agreement with published data,<sup>38</sup> the relative permittivity of the pure SPC model (system 2) is 65, which represents a relative error of 17% with respect to the experimental value of 78.4.<sup>48</sup> In line with the result obtained for the Kirkwood factors, the permittivity calculated for the hybrid system is 84, i.e., a relative error of 7% with respect to the experimental value.

We sought to characterize some dynamical features of our dual representation for liquid water. Two parameters were measured to check for the correct representation of such features, the self-diffusion coefficient and the rotational relaxation time.

Table 3 shows the value of the SPC water self-diffusion coefficient both in FG and in hybrid simulations. Coincident

with data reported in the literature,<sup>38</sup> we obtained a value of the self-diffusion coefficient in the pure FG system of  $4.3 \times 10^{-5} \text{ cm}^2/\text{s}$  as compared to the experimentally determined one of  $2.3 \times 10^{-5} \text{ cm}^2/\text{s}$ .<sup>49</sup> The same value calculated for the hybrid system presents an important reduction in the diffusion coefficient in relation with that of the FG system. Despite the difference with the atomistic value, the result of the hybrid system is closer to the experimental data.

A reasonable concern about the diffusion coefficient in the hybrid system is that the measured value could be an average resulting from two different distributions: one corresponding to SPC molecules in the FG region moving at their normal velocity and another related to SPC waters in contact or within the CG phase, which are substantially slowed down or frozen. If this were the case, the distribution of diffusion coefficients dividing the system in different subsets would be composed of two peaks, one centered at the intrinsic SPC value ( $4.3 \times 10^{-5} \text{ cm}^2/\text{s}$ ) and the other at a value even lower than the experimental one. To test this hypothesis, we calculated the distribution of the diffusion coefficient for 40 groups, each containing 50 randomly selected water molecules. The obtained distributions present only one peak (Figure S2, Supporting Information), providing evidence for a single diffusion regime, supporting a global decrease of the diffusion process of FG water in the presence of WT4.

The second parameter explored to characterize the dynamical behavior of the FG–CG mix was the rotational relaxation time, which measures the tumbling time of a molecule within a medium. It could be expected that the hybrid interface may alter the dynamical behavior of the FG water. In fact, IR spectroscopy measurements suggest that the mere presence of an interface of arbitrary nature is more important in slowing hydrogen bond dynamics than the chemical nature or geometry of this interface.<sup>50</sup> Relaxation times of water under different confining conditions show an increase from 2- to 10-fold. Table 3 lists the values obtained for both the FG and hybrid models. The SPC model underestimates the relaxation time compared to experimental values.<sup>38</sup> The values calculated for SPC in the mixture with WT4 are well in line with those for pure SPC with only a tiny increase (closer to the experimental value), indicating that WT4 molecules do not exert a confining effect on atomistic water.

Taken together, these results suggest that the presence of the CG phase introduces a small increase in the dipole–dipole correlation and relaxation time of the FG water model, which faintly slows down the diffusion of atomistic water molecules. However, the net effect of the dual representation of the liquid leads to a slightly better agreement with several experimentally determined properties.

Another important property of water is its isothermal compressibility. As reported in Table 3, we compute a value of isothermal compressibility for the hybrid system that

compares well with that of SPC<sup>51</sup> and is fairly close to the experimental one ( $0.46 \text{ GPa}^{-1}$ ). This result seems to indicate that despite the higher compressibility observed for a pure WT4 phase,<sup>24</sup> the resulting value in the hybrid system leads to a global response to external pressure fluctuations, which resembles that of the pure SPC system.

Surface tension is another key property of water and an important ingredient to drive self-assembly processes of great relevance in biology. The surface tension of the WT4 model is low ( $17 \text{ mN/m}^{24}$ ) compared to the experimental value of  $71.2 \text{ mN/m}$ .<sup>47</sup> This might raise serious concerns about the modeling of self-assembly phenomena using the hybrid solvent presented here. However, as shown in Table 3, the surface tension of the hybrid solvent calculated from system 3 is very close to the  $53.4 \text{ mN/m}$  value reported for pure SPC.<sup>37</sup> According to this analysis, WT4 molecules in the hybrid representation exert only a moderate influence on the surface tension in the FG water phase. Hence, application to biological systems should not lead to any problems. In fact, no noticeable differences between our hybrid scheme and fully atomistic simulations of membrane systems were detected (see section 3).

Finally, we calculated the heat capacity ( $C_p$ ) in order to characterize the responsiveness of the system to temperature fluctuations (Table 3).  $C_p$  was evaluated from the difference between the total energy per effective molecule at  $298 \text{ K}$  and that at  $318 \text{ K}$ . The heat capacity observed for the hybrid system underestimates the SPC and experimental ones<sup>52</sup> by  $\sim 60\%$ . This flaw is not unexpected as the hybrid system, as a whole, loses particles and degrees of freedom. This loss of entropy is reflected in the reduced capacity of the system to store thermal energy.

**2. Simple Electrolytes in Aqueous Solutions.** In this section, we will focus on the reproduction of properties related to single electrolytes in aqueous solution, as these are a fundamental component of biological systems. To assess the effectiveness of this approach, we set up a simulation system containing a 1:1 mixture of SPC/WT4 and  $0.3 \text{ M Na}^+\text{Cl}^-$  (Table 1, Figure 3A). Notice that the ionic concentration in both phases of the liquid is adjusted to be the same.

CG ions are represented as effective beads, their charge, mass, and vdW radius representing a single electrolyte implicitly carrying a first solvation shell of six waters.<sup>52</sup> Therefore, introducing CG ions within a FG aqueous medium may result in spurious interactions since the minimum distance between FG water and CG ions is smaller than the minimum distance between WT4 and CG ions. This produces a higher gain in electrostatic energy when SPC molecules solvate CG ions relative to that of WT4 solvation of CG ions. A straightforward correction for this problem is to place the FG water at the second solvation shell position by tuning the Lennard-Jones interaction between CG ions and FG water (Figure S3, Supporting Information). Such a correction is sufficient to ensure that CG ions remain in the CG phase along the MD trajectories. This can be directly observed from the averaged density across the box (Figure 3B). In close similarity with the previous section, inclusion of free electrolytes does not introduce significant differences in the partition of the FG and CG species. The density profile of FG and CG water molecules in system 3 resembles that of system 2 (Figure 2B), with a smooth transition between both phases. Analogously, the density profiles of ionic species indicate that all electrolytes remain within their respective phase. The higher oscillations in the traces of ions are very likely related to the smaller number

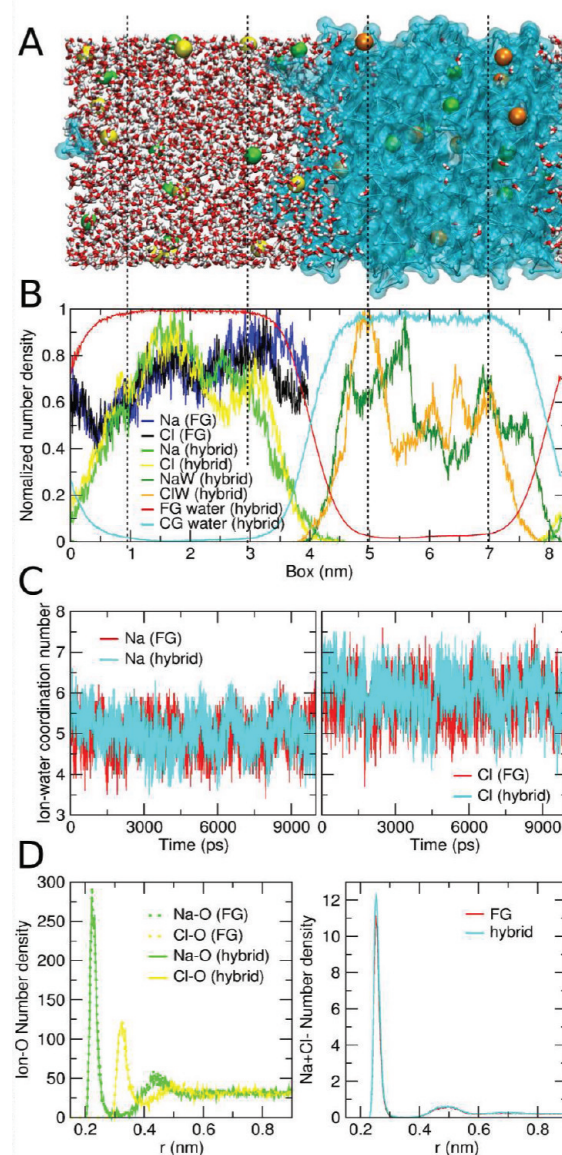


**Figure 3.** Electrolyte solution systems. (A) Snapshot of system 5 after 10 ns of molecular dynamics simulation. Red and white licorice representation, SPC water; light green and yellow vDW representation, FG  $\text{Na}^+$  and  $\text{Cl}^-$  ions, respectively; cyan CPK/surface representation, WT4; dark green and orange vDW representation, CG  $\text{NaW}^+$  and  $\text{CIW}^-$  ions, respectively. (B) Mass density profile along the direction orthogonal to the FG/CG interface for system 5. A comparison with respect to an equivalent FG simulation (system 4) is shown for reference. Vertical dashed lines indicate the limits between FG/interface and CG/interface regions. Panels A and B are on the same scale. (C) Ion–oxygen coordination number. Time series of the number of oxygen atoms at  $0.4 \text{ nm}$  from any FG ion is shown for the FG reference simulation (system 4) and the hybrid simulation (system 5). (D)  $\text{Na}-\text{oxygen}$  and  $\text{Cl}-\text{oxygen}$  number densities (left) and  $\text{Na}-\text{Cl}$  number density (right) measured on FG reference system 4 are compared against hybrid system 5.

of particles, which reduces the statistical sampling. This hypothesis is confirmed by the comparison of the traces obtained from a simulation box at the pure atomistic level (system 4), in which the amplitudes of the density oscillations are of the same magnitude (Figure 3B, left side). In contrast to water molecules, which cross the interface to a limited amount,

the penetration of FG ions into the CG phase and *vice versa* was not observed. In both cases, the density traces fall down to zero within the interface region.

Calculation of the coordination number of SPC water around  $\text{Na}^+$  and  $\text{Cl}^-$  yields indistinguishable traces for both simulation schemes (Figure 3C). Additionally, we notice that the stabilization is very rapid in both cases and happens already within the thermalization/pressurization. This observation reinforces the idea that ions display no tendency to mix. In fact, the number density curves of SPC oxygen around any of the electrolytes superimpose almost perfectly (Figure 3D, left panel). This agreement indicates that, despite the differences in electric charge and size, the perturbations that both ionic species introduce in the structure of the liquid in the hybrid and FG phases are nearly identical. This similar structure suggests that our hybrid solvation method does not modify the interactions with the solute when compared with the fully atomistic case. The good superposition of the RDFs of  $\text{Na}^+ - \text{Cl}^-$  (Figure 3D, right panel) is another strong indication of this similarity.

In analogy with the result obtained for the pure water case, the diffusion coefficients of single electrolytes in the hybrid system are underestimated with respect to the FG simulation (Table 4), the discrepancy being more notorious in the case of

**Table 4. Comparison of Physicochemical Properties of Aqueous Solutions with Free Electrolytes**

	$\text{Na}^+$ diffusion coefficient (system 4, 5) [ $\times 10^{-5} \text{ cm}^2 \text{ s}^{-1}$ ]	$\text{Cl}^-$ diffusion coefficient (system 4, 5) [ $\times 10^{-5} \text{ cm}^2 \text{ s}^{-1}$ ]	osmotic pressure (systems 6, 7) <sup>a</sup> [bar]
FG	$2.2 \pm 0.1$	$2.3 \pm 0.3$	$20 \pm 11$
hybrid	$1.1 \pm 0.2$	$1.8 \pm 0.1$	$26 \pm 11$
exptl.	$1.35 \pm 0.038^b$	$1.91 \pm 0.025^c$	$\sim 25$ (taken from <sup>39</sup> )

<sup>a</sup>Ionic concentration in systems 6 and 7 correspond to 0.5 M in the volume determined by the ion restraints. <sup>b</sup> $\text{Na}^+\text{Cl}^-$  concentration: 0.3 M.<sup>53</sup> <sup>c</sup> $\text{Na}^+\text{Cl}^-$  concentration: 0.25 M.<sup>54</sup>

$\text{Na}^+$ . However, when experimental data are taken into account, the values obtained in the FG simulation reveal an overestimated diffusional behavior, while the hybrid scheme induces a slower diffusion, as evidenced by the diffusion coefficient of both  $\text{Na}^+$  and  $\text{Cl}^-$  being closer to the experimental data. Such a decrease in the diffusion coefficient of the ions was somewhat expected, in line with the slower diffusion of water induced by the hybrid approach, as mentioned previously.

To conclude the study of free electrolytes in aqueous solution, we check that the coexistence of two phases containing electrolytes modeled with different parameters does not create an artifact in the osmotic pressure. To exclude this possibility, we calculated this quantity in a fully atomistic and a hybrid system, according to the procedure proposed by Luo and Roux.<sup>39</sup> To this aim, we constructed systems 6 and 7 (Table 1). As shown in Table 4, the average value of the osmotic pressure measured in both systems coincides well with experimental estimates, within the relatively large error intrinsic to the method.

Taken the results obtained for pure water and free electrolytes in solution together, we can expect that the solvation scheme proposed here may effectively work with more complex biomolecular systems. This hypothesis will be tested in the next section, where the simulation of a large

protein complex embedded in a double phospholipid bilayer will be addressed.

**3. SNARE Membrane Fusion Complex.** Three polypeptide chains compose the minimal SNARE fusion machinery.<sup>29</sup> This complex is constituted by three proteins, namely, synaptobrevin (SB), syntaxin (SX), and two helices of SNAP-25 (SN1 and SN2), which are associated in their cytoplasmic part by the formation of a coiled-coil four helix bundle<sup>55</sup> (Figure 1E). The association of the bundle is mediated by the recognition of conserved residues forming hydrophobic contacts on the interior sides of each protein and a series of hydrogen bonds and salt bridges (Figure 1E on the right) at the external face.<sup>56</sup> Syntaxin and synaptobrevin are anchored to the plasma and vesicular membranes, respectively. General insights into SNARE-mediated fusion from molecular simulations are reviewed in ref 57. In previous work, we have characterized the properties of separate parts of the SNARE complex. The soluble helical bundle part has been shown to act as molecular velcro, held together by specific hydrogen-bond and salt-bridge networks.<sup>56</sup> These tight interactions make it behave like a rather rigid rod, a very stiff molecular arrangement imposed by the bundle topology. The transmembrane domains show a robust insertion into the lipid bilayer, quite independent of sequence variations.<sup>5</sup> We then built a complete model of the SNARE setup shown in Figure 1D, inspired by data from AFM experiments,<sup>58</sup> suggesting that a single SNARE complex may be able to maintain two membranes at about 5 nm separation. This setup was previously equilibrated, and we use it here as starting point to compare a FG and hybrid solvation approach as a practical and highly nontrivial test case of a realistic application. We will characterize the same properties as for the individual systems in order to assess the similarity between both setups for such a complex system.

**Hybrid Simulation of the SNARE Membrane Fusion Complex.** For our investigation, we started from the equilibrated conformation after 44 ns of the previously performed MD simulation (system 8<sup>30</sup>). We extended it by 20 ns, both at the FG (system 8) and hybrid (system 9) levels of resolution. To construct the hybrid SNARE/double membrane system 9, water molecules beyond 1 nm from any solute atom were removed, and the system was resolvated with WT4 molecules. Ions within the CG region of the solute were changed to their corresponding CG version. The final configuration of system 9 is shown in Figure 4A. The first 5 ns of the 20 ns extension (from 44 to 49 ns) were used to achieve temperature, pressure, and permittivity convergence of the entire system, while the subsequent 15 ns (from 49 to 64 ns) were considered as a production run.

In close analogy with the previously analyzed cases, the hybrid solvent partitions into two regions of space separated by a smooth interface where both species coexist. An overall comparison of the density profiles between atomistic and hybrid systems suggests a good conservation of the main structural features (Figure 4B). The localization of water in the atomistic system 8 shows the expected distribution of a double membrane topology. The density level reaches maximum values in the two exterior compartments, drops in the region occupied by the lipids, and rises again in the inner compartment. The small shoulder observed on the left side of the inner slab is generated by the presence of the protein complex. Focusing on the hybrid solvent, it is apparent that SPC water is present only in the neighborhood of the membranes and protein. All of the remaining (bulk) space is filled by WT4. The sum of both SPC

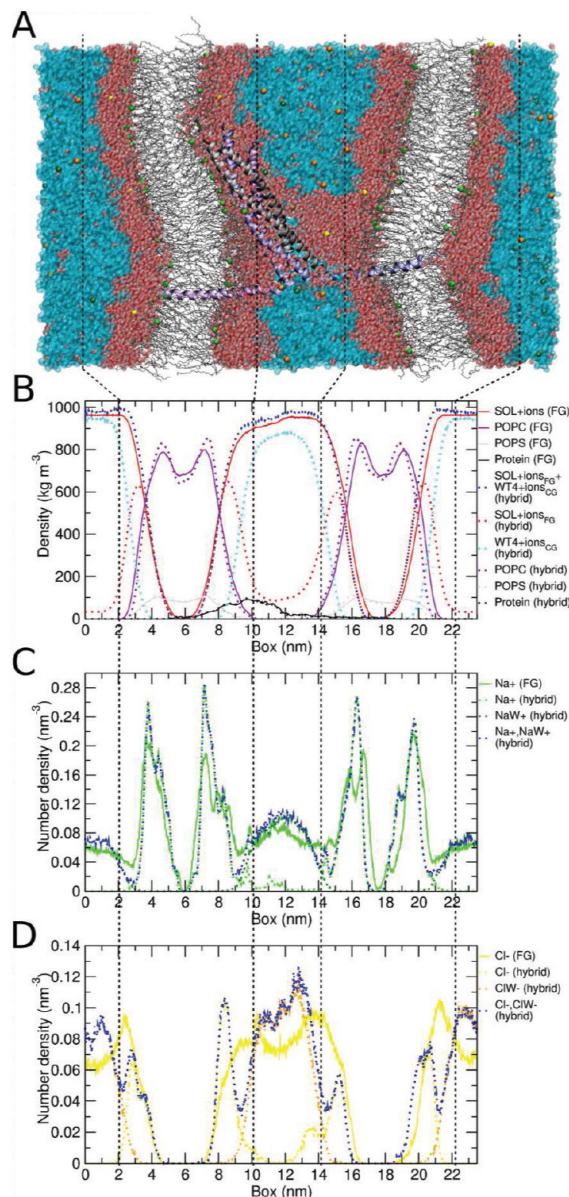


**Figure 4.** SNARE complex system (part I, density profiles). (A) Snapshot of system 9 after 20 ns of molecular dynamics simulation. Red and white vdW representation, SPC water; light green and yellow vdW representation, FG  $\text{Na}^+$  and  $\text{Cl}^-$  ions, respectively; cyan CPK/surface representation, WT4; dark green and orange vdW representation, CG  $\text{NaW}^+$  and  $\text{ClW}^-$  ions, respectively. (B) Protein, lipid, and water mass density profiles along the direction orthogonal to the membranes for system 9. (C) Sodium and (D) chloride number density profile along the direction orthogonal to the membranes for system 9. In B to D, an equivalent FG simulation (system 8) is shown for comparison. Vertical dashed lines indicate the limits between CG and interface regions; notice the change in scale between panel A and B to D.

and WT4 density profiles results in a close reproduction of the total water density measured in the purely atomistic case (Figure 4B). The difference in the observed densities results from the underestimation of the bulk mass density intrinsic to the SPC model. Small peaks of density are found near the interface, just as observed for pure water (Figure 2B). A first measure of the effect of the hybrid solvent on the global conformation of the solute can be acquired from the

comparison of the density profiles of the solutes. The density traces of the protein in both solvation schemes are nearly indistinguishable, similarly to what is observed for the profiles of the POPS phospholipids. Minor differences are only observed for the POPC molecules. This small discrepancy may be related to the averaging of long scale fluctuations in the intermembrane distance and intrinsic curvature of both membranes (see below). To overcome this problem, we selected a region of the membrane where phospholipids are not in contact with any amino acid for comparison. Calculation of the density profiles on this selected membrane patch shows a very good match between the atomistic and hybrid systems (Figure S4A, Supporting Information).

Analysis of the spatial distribution of the different electrolytes shows a rough similarity between both solvation schemes (Figure 4C). In the case of FG  $\text{Na}^+$  (Figure 4C), the cations show a marked tendency to localize at the rim of both bilayers. The distribution of cations displays defined peaks near the membrane, which can be ascribed to interactions mainly with the carbonyl groups of POPC, and to a minor extent with the phosphate moieties, and the carboxyl heads of POPS.<sup>59</sup> As the distance from the membrane increases, the  $\text{Na}^+$  density diminishes, converging to a bulk value at both sides of the membranes. On the contrary,  $\text{Cl}^-$  ions tend to localize far from the membrane owing to the repulsion with the negatively charged POPS phospholipids.<sup>60</sup> However, due to the strong localization of  $\text{Na}^+$  in the bilayer, a weak peak of  $\text{Cl}^-$  ions that remain in the nearby water phase is observed. Those  $\text{Cl}^-$  ions along with the POPS carboxyl groups counterbalance the positive charge density generated by the  $\text{Na}^+$  accumulation. Similar  $\text{Cl}^-$  localization has already been reported in the literature<sup>59,61</sup> (Figure 4D).

The ionic distribution in presence of the dual solvent (dotted lines in Figure 4C) follows the trend of its atomistic counterpart. However, as we saw in the previous section (Figure 3B), the presence of the FG–CG interface generates an electrolyte depletion in the region where both water models coexist. Unavoidably, this generates a small rise in the ion concentration in the remaining space. This effect is more pronounced in the case of  $\text{Cl}^-$ , which resides closer to the hybrid interface. In analogy with the density of POPC, the agreement with the purely atomistic system improves if the same profile is calculated on a reduced part of the system only, where the curvature is less pronounced (Figure S4B, Supporting Information). Moreover, we sought to quantify the number of contacts between ions and the different components of the systems. To this aim, we counted the average number of ions contained in a shell of 0.4 nm around lipids and proteins. Examples of ion–lipid and ion–protein interactions are shown in Figure S5, Supporting Information. As expected from Figure 4C, the largest differences are observed for the chloride–lipid contacts (Table 5). Despite

**Table 5. Comparison of Protein, Lipid, and Ion Contacts Using a 0.4 nm Distance Criterion**

	avg. number of contacts FG	avg. number of contacts hybrid
sodium–lipid	$188 \pm 4$	$192 \pm 3$
sodium–protein	$3 \pm 2$	$4 \pm 1$
chloride–lipid	$12 \pm 3$	$18 \pm 4$
chloride–protein	$3 \pm 1$	$2 \pm 1$
protein–lipid	$82 \pm 4$	$87 \pm 4$

this observation, we globally only found minor differences in the number of contacts between ions–lipids and ions–protein, which can likely be ascribed to thermal fluctuations. Nevertheless, since the adsorption of  $\text{Na}^+$  ions at the membrane border has been reported to increase the thickness by nearly 10%,<sup>62</sup> we compared this quantity in both systems to verify that no indirect effects on the membrane properties are generated. The average thickness calculated along the simulation time does not show significant differences between both solvation schemes (Figure 5A).

Due to the tension sustained by the SNARE complex, an important curvature of both membranes builds up. The intermembrane distance can be analyzed both as time-averaged 2D plots (Figure 5B) and as spatially averaged time series (Figure 5C). For the former, both simulation schemes provide the same general picture. The site of insertion of both transmembrane helices, which corresponds to the region of minimum intermembrane distance, is clearly visible near the center of both maps (Figure 5B). However, oscillations on a long multi-nanosecond time scale occur in both systems. These may lead to the small differences apparent in the intermembrane distance (Figure 5C, upper panel), affected by the somewhat arbitrary reduction of membrane oscillations and curvature related effects to a single number. It is therefore difficult to establish a precise gauge of the difference within the presently studied time scale. An exhaustive characterization of this small but sensible effect would require at least a 10-fold increase of the sampling time, which goes beyond the scope of this work. In an attempt to filter out these effects, we did analyze an alternative measure for intermembrane thickness (Figure 5C, lower panel) by using the membrane-inserted Y64 and Y164 amino acids as reference points on the protein. Much reduced discrepancies, fully within statistical fluctuations, are observed in this case.

In a further attempt to compare the membrane properties determined by both solvation schemes, we calculated some distinctive structural features of phospholipids. For the hydrophobic tails, we evaluated their order parameters, while for polar moieties we calculated the average orientation of the vector connecting the nitrogen with the phosphorus atoms in reference to the axis perpendicular to the membrane normal (P–N vectors). Since the orientation of the P–N vectors may be affected by membrane curvature, this measure was performed on the reduced bilayer patch used to calculate the POPC density profile (Figure S4, Supporting Information). Very good agreement is obtained for the average distribution of the P–N vectors in both systems (Figure 5D). Since this property strongly depends on the water/ion interaction within the polar heads, this agreement further supports the equivalence between fully atomistic and hybrid solvation strategies. Comparison between the profiles of order parameters calculated along the lipidic tails provides a similarly good agreement (Figure 5E and Figure S6, Supporting Information). Both results taken together suggest that the structure of the phospholipids remains unchanged across the entire bilayer when the hybrid scheme is applied.

In the remaining paragraphs, we focus our attention on the structure and dynamics of the protein chains present in the system. Comparison between the simulation of atomistic and hybrid systems resulted in equivalent RMSD traces, suggesting that the deviation from the starting position is nearly identical (Figure 6A). A similar profile is obtained from the evaluation of the RMS fluctuations, indicating that both protein complexes

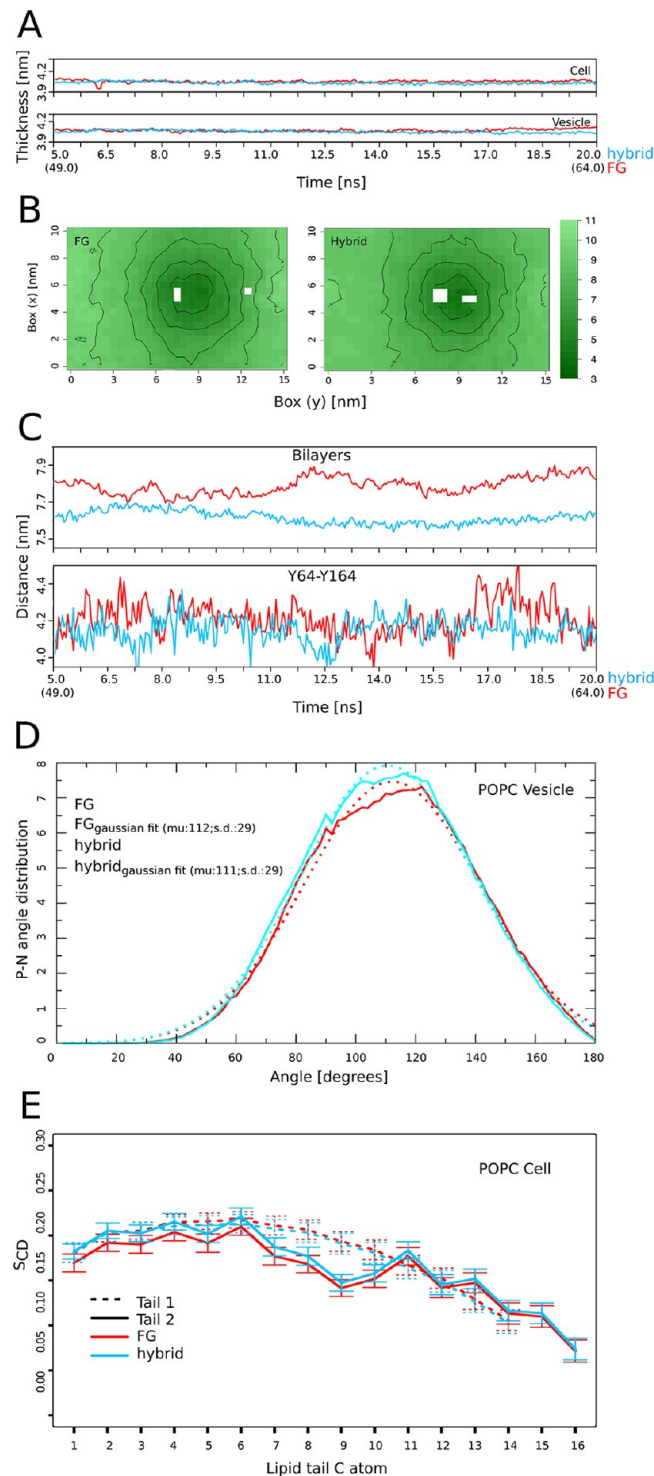


**Figure 5.** SNARE complex system (part II, membrane properties). (A) Membrane thickness vs simulation time for the cell (top) and vesicle (bottom) bilayers. Red and cyan colors are used for FG and hybrid systems, respectively. (B) Two-dimensional intermembrane distance contour plots for FG (left) and hybrid (right) systems. (C) Upper panel: Intermembrane distance time series averaged over the whole simulation box. Lower panel: Intermembrane distance estimated from the separation between residues Tyr64 (synaptobrevin) and Tyr164 (syntaxin). (D) Orientation of the POPC P–N vectors relative to the membrane normal measured on a selected membrane patch (see Computational Details section) for FG and hybrid. Dashed lines correspond to a Gaussian fit to each of the traces. (E)  $S_{CD}$  order

Figure 5. continued

parameters calculated for the POPC tails in the cell membrane (full analysis is shown in Figure S6, Supporting Information).

display a similar flexibility (Figure 6B). The largest deviations are observed within unstructured loops connecting the cytoplasmic and transmembrane helices of synaptobrevin (SB, Figure 6B), while only minor differences are present in well structured regions. The structural relevance of this higher mobility in the atomistic system can be appreciated from the superposition of 15 structures taken at 1 ns intervals along the trajectory. From a visual comparison between those conformers in the FG and hybrid systems (Figures 6C), it is clear that both simulations oscillate around similar average positions with a lower dispersion in the case of the hybrid solvent. In line with the good structural conservation, a pairwise RMSD comparison of both trajectories shows several overlapping regions, suggesting that the system explores similar configurations, but not necessarily at the same point in time (Figure S7A, Supporting Information).

These results indicate, as expected, a rather rigid conformation for the SNARE complex. Hence, we examined the underlying interactions giving rise to this rigidity by evaluating the formation of salt bridges (Figure 6D and E) and hydrogen bonds (Figure 6F). The observed pattern of interactions is very similar with some variations in the strength of individual interactions. Globally, both simulations exhibit the same level of salt-bridge mediated cohesion. The same is true for the formation of hydrogen bonds (Figure S8, Supporting Information). This observation furthermore confirms the robustness of previously highlighted interaction patterns,<sup>56</sup> even under membrane-induced tension.

A complementary view to the electrostatic interactions depicted in Figure 6D–F can be obtained by calculating the contact matrices of the complexes, which mainly account for hydrophobic contacts. Subtracting the contact matrix resulting from the hybrid simulation from the matrix of the atomistic system, we can visualize the differences in contact points, which are associated with the nonzero elements in the difference matrix. As could be anticipated from all previous results, the difference matrix is nearly zero for more than 95% of the contacts, indicating negligible differences in the interaction pattern (Supporting Information Figure S7B). Only five residues located in the terminal region of the helices show rather small deviations (below 0.25 nm), which are on the same order of magnitude as the fluctuations encountered when calculating the RMSF (Figure 6B).

Finally, we turn our attention to the protein–lipid interactions. Calculation of the number of protein–lipid contacts within 0.4 nm reveals negligible differences within the standard deviation (Table S) that can be ascribed to thermal fluctuations. Moreover, the bilayer insertion of the synaptobrevin and syntaxin transmembrane helices is indistinguishable when comparing both solvation schemes (Figure S9, Supporting Information), further hinting at the similarity of these interactions in both systems.

## CONCLUSIONS

Explicit consideration of the solvation effects in molecular systems is of fundamental relevance to achieving an atomically accurate description of biophysical processes. However, the

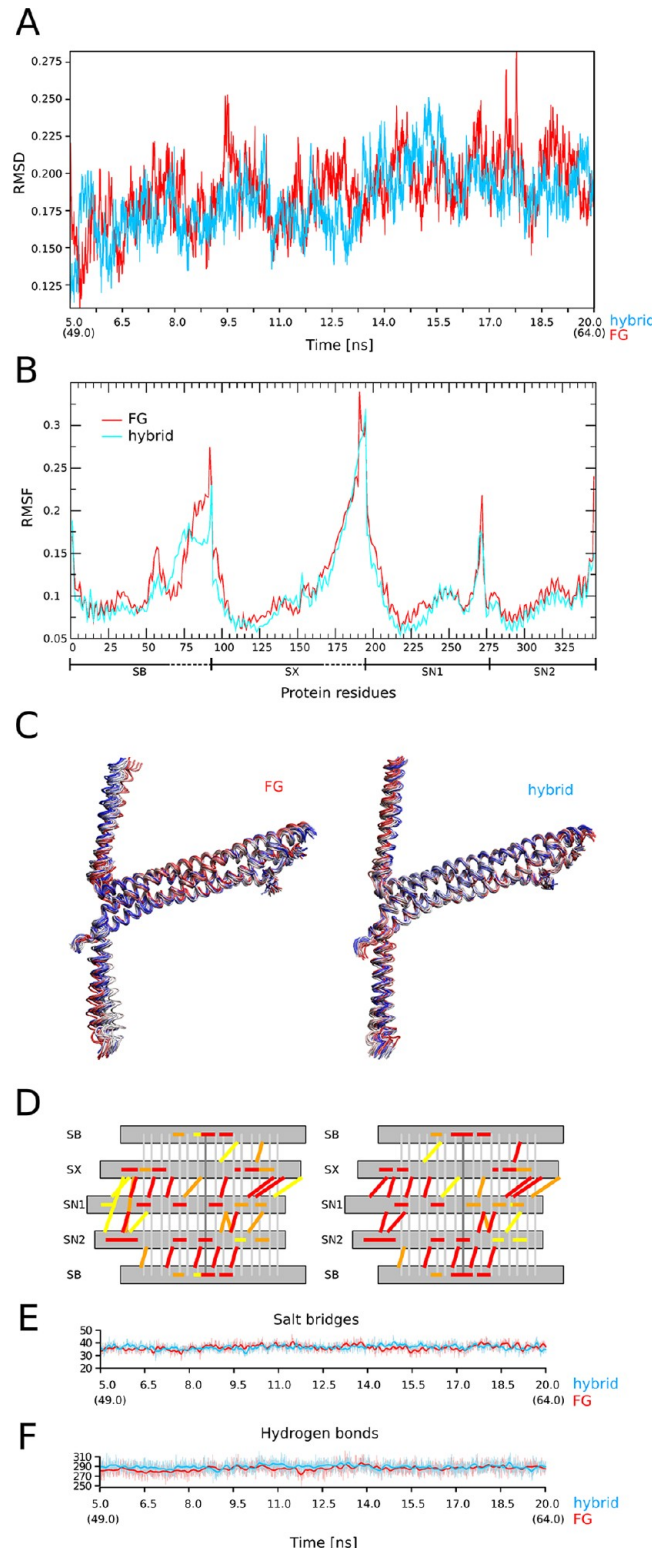


**Figure 6.** SNARE complex system (part III, protein properties). (A) RMSD time series. (B) RMS fluctuations vs residue number. The correspondence to each protein chain is indicated at the bottom. (C) RMS fit of 15 snapshots taken at 1 ns intervals for FG (left) and hybrid (right) systems. Colors vary from blue to red according to the timeline. (D) Schematic representation of salt bridges in FG and CG simulations, respectively. The color of the bars indicates the percentage of occupancy of each salt bridge during the simulation time. Yellow, orange, and red correspond to occupancies from 0% to 50%, 50% to 75%, and 75% to 100%, respectively. (E) Time series of

Figure 6. continued

the total number of salt bridge interactions. (F) Time series of the total number of hydrogen bond interactions.

very high abundance of water in biological systems imposes a serious limitation in the sizes and time scales affordable by computer simulations. The use of CG approaches represents an opportunity to tackle this problem by reducing the complexity of atomic systems at the price of a certain loss of accuracy.<sup>51</sup> Halfway between fully atomistic and CG approaches, we find hybrid or multiresolution methods, which offer an alternative to keep atomic detail in regions of interest and yet to neglect degrees of freedom in less relevant regions of the molecular systems. In this contribution, we presented a new solvation scheme which belongs to the hybrid category. We make use of the popular SPC water model in combination with the WT4 CG model for aqueous solvation previously developed by us. We show that this dual resolution solvation approach achieves a good description of physicochemical properties of pure water and electrolyte solutions. Finally, this approach is tested in a molecular system containing a trimeric protein complex inserted in a double phospholipid membrane. Systematic comparison of fully atomistic and hybrid solvation yields essentially identical results in terms of structure and dynamics of protein and membrane parts. Moreover, the interactions between different parts of the system remain unperturbed or show only minor deviations, which are compatible with thermal noise.

Clearly, the actual utility of the solvation method presented here depends on the speed-up obtained. Speed-up depends on the particular program used, computer architecture, parallelization level, etc. In the case of the SNARE system embedded in a double membrane, calculations were performed using Gromacs 4.5 on the Curie supercomputer, an x86-64-based French Tier0 system of 2 PetaFlops peak performance featuring eight-core Intel Sandy Bridge EP E5-2680 processors at 2.7 GHz. Under these conditions, the speed-up relative to the fully atomistic system varied from 30% to 49%, depending on the number of processors used (see Supporting Information Figure S10a,b). On our current Gromacs implementation, the advantage of the method resides almost exclusively in the calculation of the forces (Supporting Information Figure S10c). This benchmark result is somewhat expected as it has been recognized that MD simulations using CG models may be challenging to parallelize owing to their low density and/or inhomogeneities.<sup>63</sup> However, it is expected that future implementations may overcome these limitations. For instance, a more efficient relabeling of neighboring particles such as that reported by Meloni et al.<sup>64</sup> could be applied to our hybrid solvation system taking advantage of the slower diffusion of the CG solvent. The CG solvent neighbor list would not need to be updated as frequently as for the atomistic part. Similarly, our solvation method may highly benefit from new and promising multiple time step approaches.<sup>65</sup>

In the test cases presented here, the use of WT4 to represent bulk water leads to a reduction of 45% in the number of atoms, but this gain increases to 65% if only the cytoplasmic domain is considered.<sup>56</sup> Since the amount of atomistic water depends on the exposed surface of the solute, globular systems are more convenient than membranes. In highly solvated systems such as a bacterial ribosome,<sup>66</sup> containing about 300 000 water molecules and ions, our approach would allow for a reduction

of about 75% in system size. Other mixed approaches, such as the use of a reaction field after a given distance from the solute,<sup>67</sup> may provide a similar gain. However, these approaches are not suitable for extended systems such as biological membranes. Moreover, our hybrid approach allows for the calculation of long-range electrostatics via PME and could be used to ameliorate problems related to the interaction between periodic replicas,<sup>68</sup> since significant increases in the system's size would imply only a modest computational cost. We recently presented a hybrid model for MD simulations of DNA at two different nucleobase resolutions along a single DNA double helix.<sup>13</sup> Combination of both models would open the possibility to consider only a small region of interest, say a protein–DNA interaction region, at the fully atomistic level and the rest of a potentially very long DNA fiber with bound proteins, solvent and counterions explicitly, but at the CG level.

At the present stage, a heavy limitation of our method resides in the fact that, while water molecules may easily leave and return to the atomistic region, ions cannot. Hence, the number of atomistic ions to be included in the solvation shell must be decided at the beginning of the simulation and they will diffuse only within this portion of the space. Although this does not result in any spurious effect, it could be anticipated that this restriction may represent a particular difficulty for heavily charged surfaces or for systems involving ion permeation.

Finally, we would like to point out that the implementation of this hybrid strategy is straightforward in standard simulation packages, only requiring the interacting parameters of the WT4 molecules and CG ions, which are freely available from the authors. Moreover, since the WT4 model is based on the tetrahedral structure of water and it was developed independently of atomistic models, it could be expected to be straightforwardly compatible with other widely used water models such as TIP3P<sup>69</sup> and SPC/E.<sup>70</sup> Preliminary results obtained in our group suggest that this is, in fact, the case.

## ASSOCIATED CONTENT

### Supporting Information

Extended additional analyses of the system properties are provided. This material is available free of charge *via* the Internet at <http://pubs.acs.org>.

## AUTHOR INFORMATION

### Corresponding Author

\*Tel: +598-2522 0910 (S.P.), +33-15841-5076 (M.B.). Fax: +598-2522 0910 (S.P.), +33-15841-5026 (M.B.). E-mail: spantano@pasteur.edu.uy (S.P.), baaden@smplinux.de (M.B.).

### Notes

The authors declare no competing financial interest.

## ACKNOWLEDGMENTS

This work was performed using HPC resources from DEISA and GENCI-CINES/IDRIS (Grant 2011-071714). A.T. acknowledges support from the French Ministry of Research. This work was partially supported by ANII—Agencia Nacional de Investigación e Innovación, Programa de Apoyo Sectorial a la Estrategia Nacional de Innovación—INNOVA URUGUAY (Agreement n8 DCI – ALA/2007/19.040 between Uruguay and the European Commission).

## ■ DEDICATION

We dedicate this manuscript to the celebration of Wilfred van Gunsteren's 65th birthday to thank him for his inspiring and pioneering work in the field of molecular dynamics simulations.

## ■ REFERENCES

- (1) Hills, R. D., Jr.; Lu, L.; Voth, G. A. Multiscale coarse-graining of the protein energy landscape. *PLoS Comput. Biol.* **2010**, *6* (6), e1000827.
- (2) Klein, M. L.; Shinoda, W. Large-scale molecular dynamics simulations of self-assembling systems. *Science* **2008**, *321* (5890), 798–800.
- (3) Marrink, S. J.; Risselada, H. J.; Yefimov, S.; Tieleman, D. P.; de Vries, A. H. The MARTINI force field: coarse grained model for biomolecular simulations. *J. Phys. Chem. B* **2007**, *111* (27), 7812–7824.
- (4) Sansom, M. S.; Scott, K. A.; Bond, P. J. Coarse-grained simulation: a high-throughput computational approach to membrane proteins. *Biochem. Soc. Trans.* **2008**, *36* (Pt 1), 27–32.
- (5) Arkhipov, A.; Yin, Y.; Schulten, K. Four-scale description of membrane sculpting by BAR domains. *Biophys. J.* **2008**, *95* (6), 2806–2821.
- (6) Durrieu, M. P.; Bond, P. J.; Sansom, M. S.; Lavery, R.; Baaden, M. Coarse-grain simulations of the R-SNARE fusion protein in its membrane environment detect long-lived conformational sub-states. *Chemphyschem* **2009**, *10* (9–10), 1548–1552.
- (7) Dans, P. D.; Zeida, A.; Machado, M. R.; Pantano, S. A Coarse Grained Model for Atomic-Detailed DNA Simulations with Explicit Electrostatics. *J. Chem. Theory Comput.* **2010**, *6* (5), 1711–1725.
- (8) Nielsen, S. O.; Lopez, C. F.; Goundla, S.; Klein, M. L. Coarse grain models and the computer simulation of soft materials. *J. Phys.: Condens. Matter* **2004**, *16* (15), R418.
- (9) Orsi, M.; Essex, J. W. The ELBA force field for coarse-grain modeling of lipid membranes. *PLoS One* **2011**, *6* (12), e28637.
- (10) Ayton, G. S.; Noid, W. G.; Voth, G. A. Multiscale modeling of biomolecular systems: in serial and in parallel. *Curr. Opin. Struct. Biol.* **2007**, *17* (2), 192–198.
- (11) Matysiak, S.; Clementi, C.; Praprotnik, M.; Kremer, K.; Delle, S. L. Modeling diffusive dynamics in adaptive resolution simulation of liquid water. *J. Chem. Phys.* **2008**, *128* (2), 024503.
- (12) Neri, M.; Baaden, M.; Carnevale, V.; Anselmi, C.; Maritan, A.; Carloni, P. Microseconds dynamics simulations of the outer-membrane protease T. *Biophys. J.* **2008**, *94* (1), 71–78.
- (13) Machado, M. R.; Dans, P. D.; Pantano, S. A hybrid all-atom/coarse grain model for multiscale simulations of DNA. *Phys. Chem. Chem. Phys.* **2011**, *13* (40), 18134–18144.
- (14) Nielsen, S. O.; Bulo, R. E.; Moore, P. B.; Ensing, B. Recent progress in adaptive multiscale molecular dynamics simulations of soft matter. *Phys. Chem. Chem. Phys.* **2010**, *12* (39), 12401–12414.
- (15) Praprotnik, M.; Delle, S. L.; Kremer, K. Adaptive resolution molecular-dynamics simulation: changing the degrees of freedom on the fly. *J. Chem. Phys.* **2005**, *123* (22), 224106–224120.
- (16) Ensing, B.; Nielsen, S. O.; Moore, P. B.; Klein, M. L.; Parrinello, M. Energy Conservation in Adaptive Hybrid Atomistic/Coarse-Grain Molecular Dynamics. *J. Chem. Theory Comput.* **2007**, *3* (3), 1100–1105.
- (17) Heyden, A.; Thrular, J. Conservative algorithm for an adaptive change of resolution in mixed atomistic/coarse-grained multiscale simulations. *J. Chem. Theory Comput.* **2008**, *4*, 217–221.
- (18) Michel, J.; Orsi, M.; Essex, J. W. Prediction of partition coefficients by multiscale hybrid atomic-level/coarse-grain simulations. *J. Phys. Chem. B* **2008**, *112* (3), 657–660.
- (19) Liu, Y.; Ichiye, T. Soft Sticky Dipole Potential for Liquid Water: A New Model. *J. Phys. Chem.* **1996**, *100* (7), 2723–2730.
- (20) Shi, Q.; Izvekov, S.; Voth, G. A. Mixed atomistic and coarse-grained molecular dynamics: simulation of a membrane-bound ion channel. *J. Phys. Chem. B* **2006**, *110* (31), 15045–15048.
- (21) Izvekov, S.; Voth, G. A. A multiscale coarse-graining method for biomolecular systems. *J. Phys. Chem. B* **2005**, *109* (7), 2469–2473.
- (22) Rzepiela, A. J.; Louhivuori, M.; Peter, C.; Marrink, S. J. Hybrid simulations: combining atomistic and coarse-grained force fields using virtual sites. *Phys. Chem. Chem. Phys.* **2011**, *13* (22), 10437–10448.
- (23) Berendsen, H. J. C.; Postma, J. P. M.; van Gunsteren, W. F.; Hermans, J. *Intermolecular Forces*; Reidel: Dordrecht, The Netherlands, 1981; p 331.
- (24) Darré, L.; Machado, M. R.; Dans, P. D.; Herrera, F. E.; Pantano, S. Another Coarse Grain Model for Aqueous Solvation: WAT FOUR? *J. Chem. Theory Comput.* **2010**, *6* (12), 3793–3807.
- (25) Darré, L.; Machado, M. R.; Pantano, S. Coarse Grain Models of Water. *WIREs Comput. Mol. Sci.* **2012**, DOI: 10.1002/wcms.1097.
- (26) Pizzutti, F.; Marchi, M.; Sterpone, F.; Rossky, P. J. How protein surfaces induce anomalous dynamics of hydration water. *J. Phys. Chem. B* **2007**, *111* (26), 7584–7590.
- (27) Pomata, M. H.; Sonoda, M. T.; Skaf, M. S.; Elola, M. D. Anomalous dynamics of hydration water in carbohydrate solutions. *J. Phys. Chem. B* **2009**, *113* (39), 12999–13006.
- (28) Laage, D.; Hynes, J. T. A molecular jump mechanism of water reorientation. *Science* **2006**, *311* (5762), 832–835.
- (29) Sollner, T.; Whiteheart, S. W.; Brunner, M.; Erdjument-Bromage, H.; Geromanos, S.; Tempst, P.; Rothman, J. E. SNAP receptors implicated in vesicle targeting and fusion. *Nature* **1993**, *362* (6418), 318–324.
- (30) Krieger, E.; Leger, L.; Durrieu, N.; Taib, P.; Bond, P.; Laguerre, R.; Lavery, R.; Sansom, M. S.; Baaden, M. Atomistic modeling of the membrane-embedded synaptic fusion complex: a grand challenge project on the DEISA HPC infrastructure. In *Parallel Computing: Architectures, Algorithms and Applications*; Joubert, C. B. G. R., Peters, T., Lippert, T., Buecker, B., Gibbon, B., Mohr, B., Eds.; John von Neumann Institute for Computing: Juelich, Germany, 2007; Vol. 38, pp 729–736.
- (31) Hess, B.; Bekker, H.; Berendsen, H. J. C.; Fraaije, J. LINCS: A linear constraint solver for molecular simulations. *J. Comput. Chem.* **1997**, *18* (12), 1463–1472.
- (32) Miyamoto, S.; Kollman, P. A. Settle: An analytical version of the SHAKE and RATTLE algorithm for rigid water models. *J. Comput. Chem.* **1992**, *13* (8), 952–962.
- (33) Berendsen, H. J. C.; Postma, J. P. M.; van Gunsteren, W. F.; Dinola, A.; Haak, J. R. Molecular-Dynamics with Coupling to an External Bath. *J. Chem. Phys.* **1984**, *81* (8), 3684–3690.
- (34) Darden, T.; York, D.; Pedersen, L. Particle mesh Ewald - an  $N \log(N)$  method for Ewald sums in large systems. *J. Chem. Phys.* **1993**, *98* (12), 10089–10092.
- (35) Essman, U.; Perera, L.; Berkowitz, M.; Darden, T.; Lee, H.; Pedersen, L. A smooth particle mesh Ewald method. *J. Chem. Phys.* **1995**, *103* (19), 8577–8593.
- (36) Herrero, C. P. Compressibility of solid helium. *J. Phys.: Condens. Matter* **2008**, *20* (29), 295230–295239.
- (37) Chen, F.; Smith, P. E. Simulated surface tensions of common water models. *J. Chem. Phys.* **2007**, *126* (22), 221101–221103.
- (38) Yu, H. B.; Hansson, T.; van Gunsteren, W. F. Development of a simple, self-consistent polarizable model for liquid water. *J. Chem. Phys.* **2003**, *118* (1), 221–234.
- (39) Luo, Y.; Roux, B. Simulation of osmotic pressure in concentrated aqueous salt solution. *J. Phys. Chem. Lett.* **2010**, *1*, 183–189.
- (40) van Gunsteren, W. F.; Berendsen, H. J. C. *Gromos-87 Manual*; Biomas BV: Groeningen, The Netherlands, 1987.
- (41) Mukhopadhyay, P.; Monticelli, L.; Tieleman, D. P. Molecular dynamics simulation of a palmitoyl-oleoyl phosphatidylserine bilayer with  $\text{Na}^+$  counterions and  $\text{NaCl}$ . *Biophys. J.* **2004**, *86* (3), 1601–1609.
- (42) Vermeer, L. S.; de Groot, B. L.; Reat, V.; Milon, A.; Czaplicki, J. Acyl chain order parameter profiles in phospholipid bilayers: computation from molecular dynamics simulations and comparison with  $^2\text{H}$  NMR experiments. *Eur. Biophys. J.* **2007**, *36* (8), 919–931.
- (43) Neumann, M. Computer simulation and the dielectric constant at finite wavelength. *Mol. Phys.* **1986**, *57* (1), 97–121.

- (44) Ludwig, R. NMR relaxation studies in water-alcohol mixtures: the water-rich region. *Chem. Phys.* **1995**, *329* (1–3), 329–337.
- (45) Fernandez, D. P.; Mulev, Y.; Goodwin, A. R. H.; Levelt Sengers, J. M. H. A Database for Static Dielectric Constant of Water and Steam. *J. Phys. Chem. Ref. Data* **1995**, *24*, 33–71.
- (46) Eisenberg, D.; Kauzmann, W. *The Structure and Properties of Water*, 2nd ed.; Oxford University Press: Oxford, U. K., 1969; pp 1–308.
- (47) Dilmohamud, B. A.; Seenevassan, J.; Rughooputh, S. D. D. V.; Ramasami, P. Surface tension and related thermodynamic parameters of alcohols using the Traube stalagmometer. *Eur. J. Phys.* **2005**, *26* (6), 1079–1084.
- (48) Murrell, J. N.; Jenkins, A. D. *Properties of Liquids and Solutions*, 2nd ed.; John Wiley & Sons: Chichester, U. K., 1994.
- (49) Krynicki, K.; Green, C. D.; Sawyer, D. W. Pressure and temperature dependence of self-diffusion in water. *Faraday Discuss. Chem. Soc.* **1978**, *66*, 199–208.
- (50) Fayer, M. D. Dynamics of water interacting with interfaces, molecules, and ions. *Acc. Chem. Res.* **2012**, *45* (1), 3–14.
- (51) Wang, H.; Junghans, C.; Kremer, K. Comparative atomistic and coarse-grain study of water: what do we lose by coarse-graining. *Eur. Phys. J. E* **2009**, *28*, 221–229.
- (52) Kuo, I.-F. W.; Mundy, C. J.; McGrath, M. J.; Siepmann, J. I.; VandeVondele, J.; Sprik, M.; Hutter, B.; Chen, M.; Klein, M. L.; Mohamed, M.; Kack, M.; Parrinello, M. Liquid water from first principles: Investigation of different sampling approaches. *J. Phys. Chem. B* **2004**, *108*, 12990–12998.
- (53) Wang, J. H.; Miller, S. Tracer-diffusion in Liquids. II. The Self-diffusion as Sodium Ion in Aqueous Sodium Chloride Solutions. *J. Am. Chem. Soc.* **1952**, *74* (6), 1611–1612.
- (54) Wang, J. H. Tracer-diffusion in Liquids. III. The Self-diffusion as Sodium Ion in Aqueous Sodium Chloride Solutions. *J. Am. Chem. Soc.* **1952**, *74* (6), 1612–1615.
- (55) Chen, X.; Tomchick, D. R.; Kovrigin, E.; Arac, D.; Machius, M.; Sudhof, T. C.; Rizo, J. Three-dimensional structure of the complexin/SNARE complex. *Neuron* **2002**, *33* (3), 397–409.
- (56) Durrieu, M. P.; Lavery, R.; Baaden, M. Interactions between neuronal fusion proteins explored by molecular dynamics. *Biophys. J.* **2008**, *94* (9), 3436–3446.
- (57) Risselada, H. J.; Grubmuller, H. How SNARE molecules mediate membrane fusion: recent insights from molecular simulations. *Curr. Opin. Struct. Biol.* **2012**, *22* (2), 187–196.
- (58) Yersin, A.; Hirling, H.; Steiner, P.; Magnin, S.; Regazzi, R.; Huni, B.; Huguenot, P.; De los, R. P.; Dietler, G.; Catsicas, S.; Kasas, S. Interactions between synaptic vesicle fusion proteins explored by atomic force microscopy. *Proc. Natl. Acad. Sci. U. S. A* **2003**, *100* (15), 8736–8741.
- (59) Jurkiewicz, P.; Cwiklik, L.; Vojtiskova, A.; Jungwirth, P.; Hof, M. Structure, dynamics, and hydration of POPC/POPS bilayers suspended in NaCl, KCl, and CsCl solutions. *Biochim. Biophys. Acta* **2012**, *1818* (3), 609–616.
- (60) Herrera, F. E.; Pantano, S. Structure and dynamics of nano-sized raft-like domains on the plasma membrane. *J. Chem. Phys.* **2012**, *136* (1), 015103–015114.
- (61) Bockmann, R. A.; Hac, A.; Heimburg, T.; Grubmuller, H. Effect of sodium chloride on a lipid bilayer. *Biophys. J.* **2003**, *85* (3), 1647–1655.
- (62) Herrera, F. E.; Pantano, S. Salt induced asymmetry in membrane simulations by partial restriction of ionic motion. *J. Chem. Phys.* **2009**, *130* (19), 195105–195114.
- (63) van der Spoel, D.; Hess, B. Gromacs - the road ahead. *WIREs Comput. Mol. Sci.* **2011**, *1* (5), 710–715.
- (64) Meloni, S.; Rosati, M.; Colombo, L. Efficient particle labeling in atomistic simulations. *J. Chem. Phys.* **2007**, *126*, 121102–121106.
- (65) Omelyan, I.; Kovalenko, A. Interpretation of atomic motion in flexible molecules: Accelerating of molecular dynamics simulations. *Phys. Rev. E* **2012**, *85*, 026706–026722.
- (66) Yam, W. K.; Wahab, H. A. Molecular insights into 14-membered macrolides using the MM-PBSA method. *J. Chem. Inf. Model.* **2009**, *49* (6), 1558–1567.
- (67) Petraglio, G.; Ceccarelli, M.; Parrinello, M. Nonperiodic boundary conditions for solvated systems. *J. Chem. Phys.* **2005**, *123* (4), 044103–044110.
- (68) Hunenberger, P. H.; McCammon, J. A. Effect of artificial periodicity in simulations of biomolecules under Ewald boundary conditions: a continuum electrostatics study. *Biophys. Chem.* **1999**, *78* (1–2), 69–88.
- (69) Jorgensen, W. L.; Chandrasekaran, R.; Madura, J. D.; Impey, R. W.; Klein, M. L. Comparison of simple potential functions for simulating liquid water. *J. Chem. Phys.* **1983**, *79*, 926–935.
- (70) Berendsen, H. J. C.; Grigera, J. R.; Straatsma, T. P. The Missing Term in Effective Pair Potentials. *J. Phys. Chem.* **1987**, *91*, 6269–6271.
- (71) Chavent, M.; Vanel, A.; Tek, A.; Levy, B.; Robert, S.; Raffin, B.; Baaden, M. GPU-accelerated atom and dynamic bond visualization using hyperballs: a unified algorithm for balls, sticks, and hyperboloids. *J. Comput. Chem.* **2011**, *32* (13), 2924–2935.